Journal of Materials Chemistry

Cite this: *J. Mater. Chem.*, 2012, **22**, 22290

www.rsc.org/materials

PAPER

Synthesis of polypeptide conjugated with near infrared fluorescence probe and doxorubicin for pH-responsive and image-guided drug delivery†

Tao Xing,[a] Xianzhu Yang,[b] Feng Wang,[b] Bin Lai[a] and Lifeng Yan*[a]

Received 19th August 2012, Accepted 5th September 2012
DOI: 10.1039/c2jm35627a

A near infrared fluorescent polymeric drug delivery system (NIRF DDS) with pH-responsive drug release properties has been designed and developed. This material was prepared by chemical conjugation of the anticancer drug doxorubicin and hydrophobic aminocyanine dye to triblock copolypeptide *via* hydrazone and amide bonds, respectively. Conjugation with aminocyanine shows almost no toxicity of the material, while conjugation with doxorubicin induces pronounced toxicity on the original biocompatible material. The pH sensitive drug release nature of the near infrared fluorescent polymeric drug (NIRF prodrug) was confirmed by accelerated drug release at pH of 5.0 *via* an *in vitro* drug release experiment and gradual drug cleavage from the NIRF prodrug during a confocal laser scanning microscopic (CLSM) experiment. The CLSM experiment also reveals that the released drug subsequently migrated to the nucleus, while the polymeric residue still remained in cytoplasm, indicating that the as-prepared polymer can be a promising candidate for theranosis of cancer.

Introduction

For cancer treatment, both its early stage diagnosis and subsequent therapy go a long way to minimize the danger.[1] The term "theranosis" has therefore been coined to describe a combination of these two functionalities.[2,3] Polymeric nanoparticles emerge as potential theranostic systems for future cancer treatment due to their versatility in both structure and functionality.[4–6] The nano-sized nature of these systems allows for a longer blood circulation time and provides shelter for the loaded theranostic agents. Besides, as a result of the highly permeable vascular structure of tumor tissue induced by rapid and abnormal angiogenesis, as well as a dys-functional lymphatic drainage, these nanoparticles were found to preferentially accumulate at the position of the tumor *via* an enhanced permeability and retention (EPR) mechanism,[7] thus reducing its non-specific accumulation, either related to diagnosis or therapy.

Diagnosis of cancer in its early stage is of vital importance for its subsequent treatment. Various tumor imaging methods based on different imaging modalities have been developed for this purpose: metallic or magnetic compounds such as iron oxide for magnetic resonance imaging (MRI),[8,9] radioisotopes for positron emission tomography (PET),[10] or fluorescent chemical agents such as quantum dots[11–13] and organic dyes[14–16] for optical imaging. Optical imaging is a widely used method both for *in vivo* and *in vitro* imaging, because of the commercial availability of organic dyes and the relatively low cost of detection. However, imaging with visible light suffers from a series of problems such as low penetration (2–3 cm), pronounced background auto-fluorescence, severe tissue absorption and scattering. Low depth penetration of visible light reduces the detection availability and greatly limits its use in living body imaging. Imaging in the near infrared region (700–900 nm), on the other hand, eliminates undesired background noises and thus becomes a more valid method for *in vivo* imaging.[17,18]

Chemotherapy is a effective method for tumor treatment, but its application has been restricted due to the lack of an effective drug delivery method to tumor tissue. Small drug molecules normally could not reach the tumor tissue efficiently, because of the inherent physiological barriers such as blood component interaction. Nonspecific distribution of the administrated drugs in biological systems not only results in unwanted drug waste, but also leads to much more serious problems, usually resulting from its pronounced toxicity to normal tissue. The emergence of nanoparticles offers new methods of drug administration; physically or chemically loaded drugs in nanoparticles could reduce drug loss during blood circulation, thus increasing drug use efficiency.[19,20] The development of intelligent nano-particles,[21–24] which could release a loaded drug under environmental stimuli, further optimizes the drug performance *in vivo*. Usually, the drug can either be physically loaded into

[a]*Department of Chemical Physics, Hefei National Laboratory for Physical Sciences at the Microscale, University of Science and Technology of China, Hefei, 230026, P. R. China. E-mail: lfyan@ustc.edu.cn; Fax: +86-551-3606853*
[b]*School of Life Science, University of Science and Technology of China, Hefei, 230026, P. R. China*

† Electronic supplementary information (ESI) available: Mass spectra of compounds **4** and **5**, CLSM images of free doxorubicin after 8 h. See DOI: 10.1039/c2jm35627a

environmental stimulus responsive nanoparticles,[25,26] or chemically bonded to non-responsive nanoparticles *via* a responsive chemical bond,[27–29] while a combination of the above two methods may be more optimal. pH[25,29] and reduction[30,31] are the two most utilized stimuli for controlled drug delivery. The design rationale of reduction sensitive nanocarriers lies in the fact that glutathione, which acts as a reducing agent to cleave disulfide linkage, was of a concentration several orders higher inside than outside the cell.[30] Cleavage of the disulfide bond stabilized nanoparticle usually leads to partial or total disassembly of the nanocarrier, activating the release of the embedded drug. pH-responsive nanoparticles were developed on the basis of the more acidic nature of the tumor cell. The lower local pH of the tumor microenvironment was partially induced by the elevated rates of glucose uptake but reduced rates of oxidative phosphorylation, while insufficient blood supply and poor lymphatic drainage are the other two factors contribute to this microenvironmental acidity.[32] pH-responsive nanoparticles thus developed are required to be stable at physiological pH (7.0), but undergo chemical bond cleavage and drug release activation under acid conditions (pH = 5.0). The pH-responsive nanoparticle can be designed either as a pH-responsive nanoparticle with a physically loaded drug, or a polymeric drug (prodrug) where the drug is chemically attached to the nanoparticle *via* a pH sensitive bond. A chemically bonded drug may be more optimal because of the firmer connection between the nanoparticle and the drug, which further reduces undesired drug leakage during delivery. One notable example was the attachment of the anticancer drug doxorubicin to hydrazine containing copolymers *via* the hydrazone bond; hydrolysis of the hydrazone linkage under acidic conditions leads to activation of the originally dormant drug delivery system.[28,33]

Combined NIRF cyanine dye with a responsive drug-conjugated nanoparticle can be a useful method for tumor theranosis. With the aid of a NIRF cyanine dye, the accumulation behavior of the nanoparticle could be conveniently monitored *in vivo*. Due to the EPR effect directed nanoparticle accumulation, the cyanine signal is also hoped to accumulate at the tumor site during blood circulation. Tumor imaging could thus be realized without using the usually complicated modified cyanine molecules with tumor-targeting abilities.[34–36] Cyanine dye can be incorporated into the nanoparticle *via* physical encapsulation[6] or chemical conjugation,[37,38] while chemical conjugation is a much more suitable method since the separation of the two is no longer possible because of a firmer linkage between them. Besides, non-specific accumulation of free dye is also no longer possible and information related with tumor diagnosis form the fluorescent nanoparticle is much more reliable. Both hydrophobic and hydrophilic cyanine molecules could be used for nanoparticle conjugation; hydrophilic cyanine dye usually contains multi-sulfonic acid groups to improve its water solubility, and the purification of those high polar molecules was usually very difficult while the yields remained low. On the other hand, hydrophobic dyes are much easier to obtain with satisfactory yields, usually *via* normal phase column chromatography. Thus, labeling with hydrophobic cyanine molecules may be a more promising method for tumor imaging.

Here, we report the synthesis of a novel pH-responsive drug delivery system with near infrared fluorescence (NIRF DDS) for anticancer drug doxorubicin delivery (Scheme 1). Schematic illustrations of the material synthesis were shown in Schemes 2 and 3. Triblock copolymer mPEG-PAsp-PZLLys **2** was prepared in the first place by sequential ring opening polymerization of aspartic acid β-benzyl ester *N*-carboxy anhydride (Asp-NCA) and ε-carbobenzoxy-L-lysine NCA (ZLLys-NCA) by amino terminated poly(ethylene glycol) methyl ether (mPEG-NH_2). Aminolysis of the side β-benzyl ester group with hydrazine dihydrochloride leads to the formation of hydrazine functionalized triblock copolymer **3**. Doxorubicin was then attached to the side chain of the copolymer *via* a pH sensitive hydrazone bond to prepare prodrug **7**. Heptamethine cyanine dye **5** was attached to the prodrug **7** *via* an amide bond to prepare NIRF prodrug **8**. Micellization of the above NIRF prodrug into water leads to the formation of NIRF DDS, with both drug delivery and diagnostic abilities. Combining both the pH-responsive drug release ability and the near infrared optical properties, the material synthesized here can be a paradigm for future theranostic agent synthesis, while the conjugation of nanoparticles with hydrophobic cyanine dye can be a useful tip for future fluorescent NIRF nanoparticle synthesis.

Results and discussion

Dye synthesis

Detailed synthetic procedures of cyanine **4** have been reported elsewhere.[36] Inserting a rigid cyclohexenyl ring into the polymethine chain of cyanine was found to be a valuable method for its functionalization, in that it both increases the dye stability and provides a useful site for further functionalization.[39] A chlorine atom located on the *meso*-position of the central ring could be substituted by various nucleophilic regents such as amine,[38,40] thiol[41] and alcohol,[36] while alcohol and thiol substitutions show no significant influence on the optical properties. Amine substitution leads to the formation of aminocyanine, which was found to improve the dye stability and optical properties simultaneously.[40] Both the absorption and emission of aminocyanine shift to shorter wavelengths and a large Stokes shift was observed. The large Stokes shift of the resulting aminocyanine was assumed to be induced by intramolecular charge transfer (ICT), which is also reflected by the break in the mirror image relationship between the absorption and emitting curves. The large Stokes shift minimizes self-quenching of these dye molecules and helps to improve their quantum yield. The maximum absorption and emission wavelengths of dye **4** are 780 and 815 nm in methanol, while they are 650 and 780 nm for dye **5**. Blue shifts of the absorption and emission could be attributed to the ICT effect.

The obtained cyanine **4** and **5** were thoroughly characterized, and mass spectra of **4** and **5** were shown in Fig. S1 and S2.† In both cases the related molecular cation peak $[M-Br^-]^+$ could be observed.

Synthesis of hydrazine functionalized triblock copolymer

Triblock copolymer **2** was synthesized by sequential ring opening polymerization of Asp-NCA and ZLLys-NCA with mPEG–NH_2, as shown in Scheme 2. To avoid side reactions associated with NCA polymerization at elevated temperatures,[42] the present

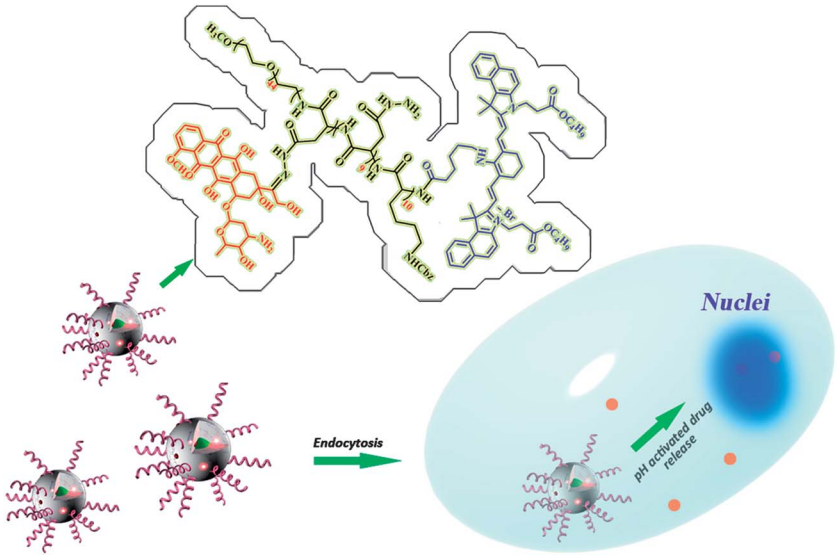

Scheme 1 Endocytosis of the NIRF prodrug micelle and its subsequent pH triggered drug release.

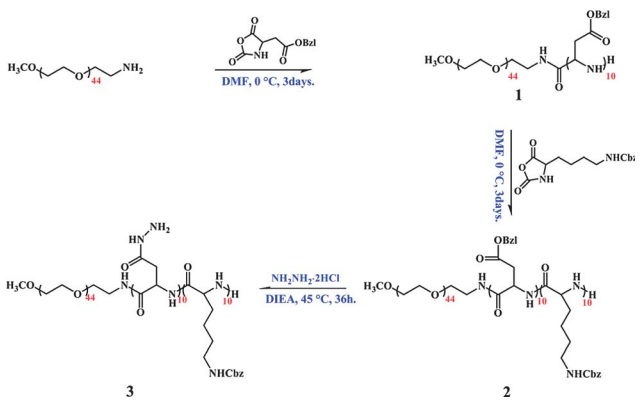

Scheme 2 Synthesis of triblock copolymer **3** by sequential ring opening polymerization.

polymerization was conducted at 0 °C. Diblock copolymer mPEG-PAsp **2** was obtained after stirring the solution at 0 °C for 3 days. 1 mL solution was removed and the product was separated from the solution for analysis. The ^{1}H NMR spectrum of the diblock copolymer (mPEG-PAsp) was shown in Fig. 1, and chemical shifts corresponding to the mPEG moiety could be observed at 3.23 ppm (CH_3O–) and 3.50 (–CH_2CH_2O–) ppm. Signals at 5.02 ($C_6H_5CH_2$–) ppm and 7.28 ($C_6H_5CH_2$–) ppm could be assigned to the benzyl ester group of the PAsp moiety. The protons of the side methylene group could be observed at 2.82 and 2.61 (–CH_2–OBzl) ppm. The chemical composition of the copolymer was determined by the integration ratio of the respective proton peak. The integration ratio of peak c (methylene group of mPEG backbone) to peak e (benzyl group of OBzl group) was calculated to be 172 : 50, which is quite close to the theoretical value 176 : 50, indicating the formation of the desired diblock copolymer. To simplify the synthesis, ZLLys-NCA was added after the consumption of Asp-NCA. The reaction was stirred at 0 °C for another 3 days. The ^{1}H NMR spectrum of the obtained triblock copolymer was shown in Fig. 2. Except for signals corresponding to diblock copolymer **2**, new chemical shifts corresponding to the PZLLys moiety are observed. Chemical shifts centered at 1.40 (–$(CH_2)_3$–Cbz) ppm correspond to the side methylene chain of PZLLys; the carbobenzoxy group of ZLLys could be observed at 5.02 ($C_6H_5CH_2$–) and 7.25 ($C_6H_5CH_2$–) ppm, which partially overlapped with the signals of the PAsp moiety. The chemical composition of the triblock copolymer could also be determined by ^{1}H NMR. The integration ratio of peak a + b + c (corresponding to the side methylene groups of PZLLys, Fig. 2) to peak f (corresponding to the methylene group of the mPEG backbone) was calculated to be 170 : 60, which is also close to the theoretical value of 176 : 60, indicating the formation of the targeted triblock copolymer. GPC traces of both the diblock and triblock were shown in Fig. 3, and a shift toward higher molecular weight (corresponding to lower retention time) was observed after each addition of monomer. Both the peaks were single and no shoulder peak corresponding to the diblock copolymer could be observed on the triblock copolymer trace, indicating that no dead polymer chains were created during diblock copolymerization. The living nature of the polymerization could be attributed to the fact that the present polymerization was conducted at low temperature (0 °C). Side reactions were thus greatly suppressed.[42]

Molecular weights and polydispersity indexes (PDI) of both the diblock and triblock copolymer were evaluated by GPC, and the results were listed in Table 1, entries 1 and 2, respectively. Molecular weights calculated by ^{1}H NMR integration were also presented as references. In both cases a difference between the two molecular weights could be observed, this is due to the polystyrene standards used for molecular weight calibration.[43]

For the preparation of hydrazine functionalized triblock copolymer **3**, the side benzyl ester group of the PAsp moiety was substituted by hydrazine dihydrochloride. Complete substitution was confirmed by the ^{1}H NMR spectrum shown in Fig. 4. Due to the signal overlap of the OBzl group with the Cbz group of the PZLLys moiety, direct observation of the disappearance of the

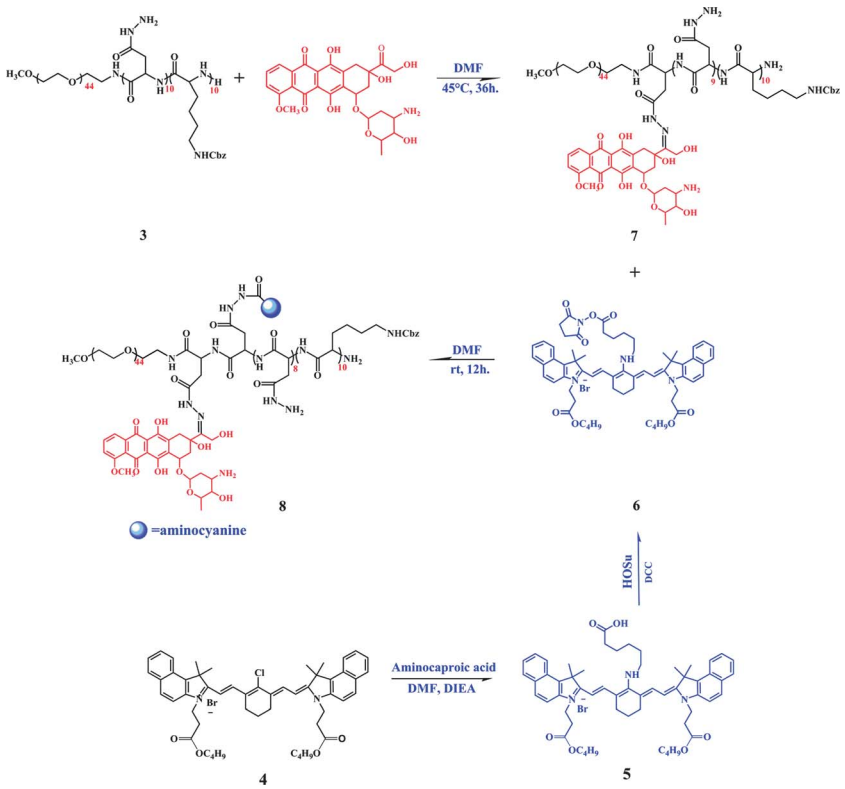

Scheme 3 Synthesis of NIRF prodrug.

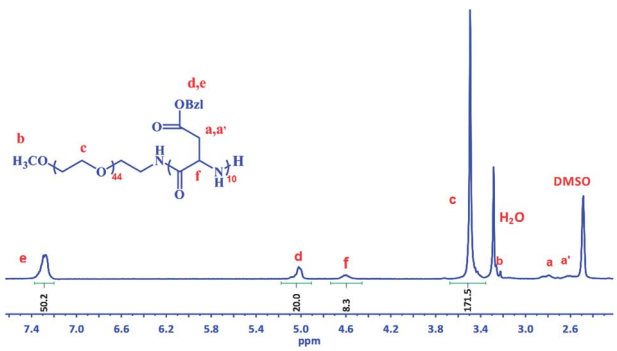

Fig. 1 ^{1}H NMR spectrum of diblock copolymer **1** in DMSO-d_6.

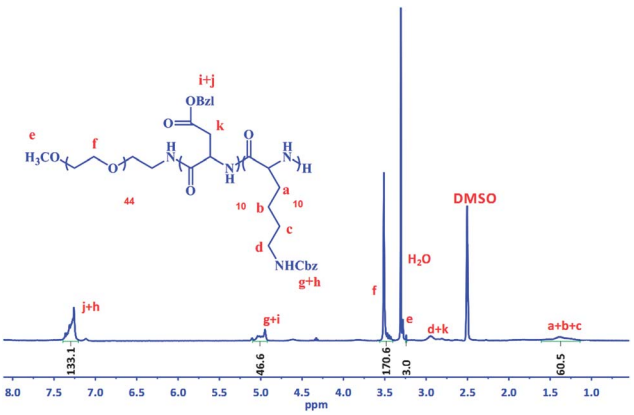

Fig. 2 ^{1}H NMR spectrum of triblock copolymer **2** in DMSO-d_6.

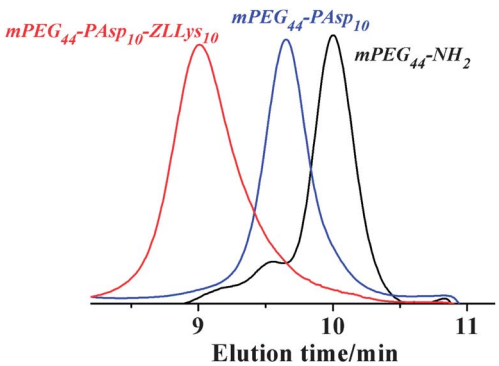

Fig. 3 GPC traces of the diblock copolymer and triblock copolymer in DMF; macroinitiator mPEG–NH_2 was also presented as a reference.

Table 1 Molecular weights and polydispersity indexes of the obtained diblock and triblock copolymer

Sample	$M_n^{NMR a}$	$M_n^{GPC b}$	M_w/M_n^{GPC}
$mPEG_{44}$-$PAsp_{10}$	3952	5458	1.04
mPEG-$PAsp_{10}$-$PZLLys_{10}$	6572	9459	1.10

[a] Molecular weight determined by ^{1}H NMR integration. [b] Molecular weight determined by GPC.

characteristic signals of the benzyl ester group is not possible. However, the substitution could be evaluated by integration into the ^{1}H NMR spectrum. The integration ratio of peak h (benzyl group of the PZLLys moiety) to peak d (methylene group

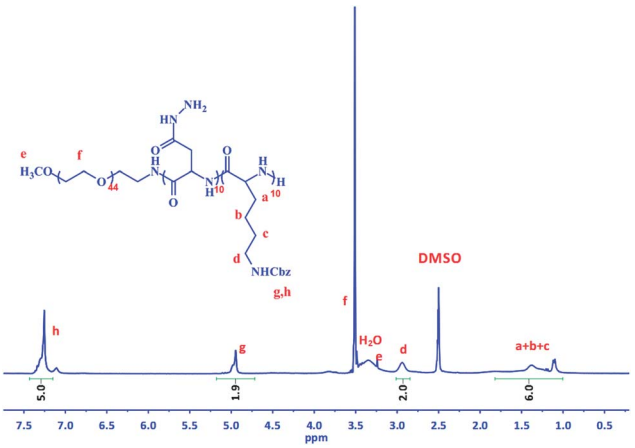

Fig. 4 ^{1}H NMR spectrum of hydrazine functionalized triblock copolymer **3** in DMSO-d_6.

adjacent to Cbz protected amine group of PZLLys) was 5 : 2 after reaction, which corresponds to the composition of PZLLys, indicating the full removal of OBzl from the side chain of the triblock copolymer.

Synthesis of prodrug 7

Doxorubicin was attached to the side chain of the above hydrazine functionalized triblock copolymer by a condensation reaction between the two, shown in Scheme 3. The condensation of the carbonyl group with the hydrazine group yields drug–polymer conjugates *via* a pH sensitive hydrazone bond. However, the ^{1}H NMR spectrum of the prodrug is poorly resolved, and proton signals corresponding to the doxorubicin moiety are not visible in the ^{1}H NMR spectrum of the prodrug, even at a sample concentration of 10 mg mL^{-1} (data not shown),

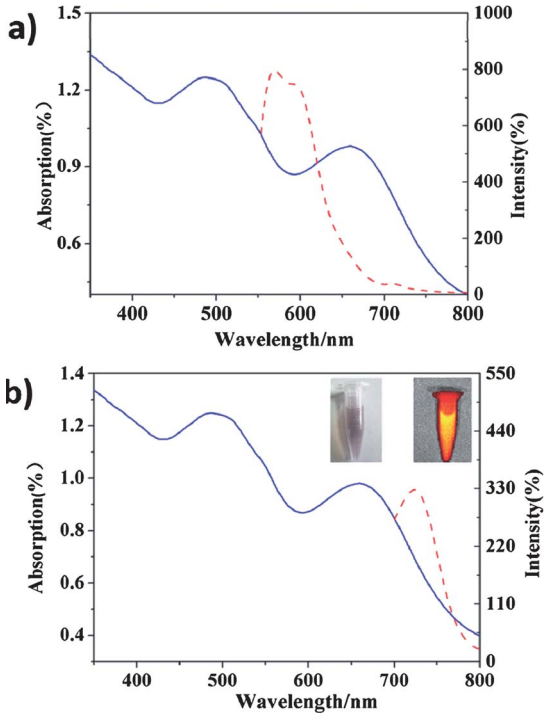

Fig. 6 Absorption (solid line) and emission (dashed line) curves of the NIRF prodrug micelle solution (0.8 mg mL^{-1}). (a) Excited at 480 nm. (b) Excited at 650 nm; the excitation and emission slit widths were 5 and 15 nm, respectively. The insets of b are images of the NIRF prodrug micelle solution and its fluorescent image upon excitation at 670 nm.

and this may be due to the fact that a low drug content (8.6%, weight ratio) was conjugated. Quantification of the drug conjugation ratio was thus evaluated by fluorospectrophotometry after treating the NIRF prodrug solution with 2 M concentrated hydrochloride aqueous solution after 1 h. The drug conjugated to

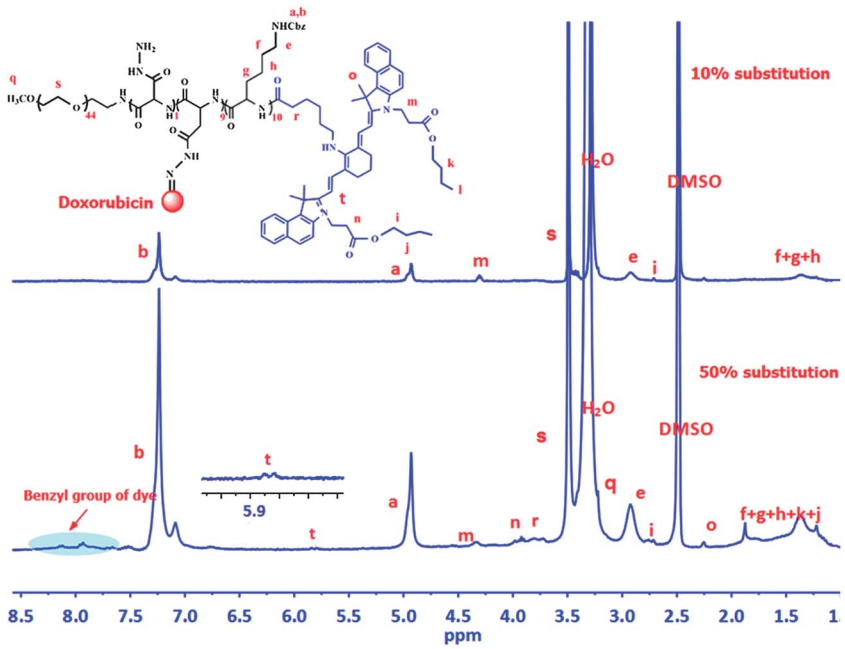

Fig. 5 ^{1}H NMR spectrum of NIRF prodrug **8** with 10% and 50% dye substitution in DMSO-d_6.

Table 2 Quantum yields of the NIRF prodrug at different degrees of aminocyanine substitution

Substitution	10%	25%	50%
Φ_f	0.0250	0.0199	0.0074

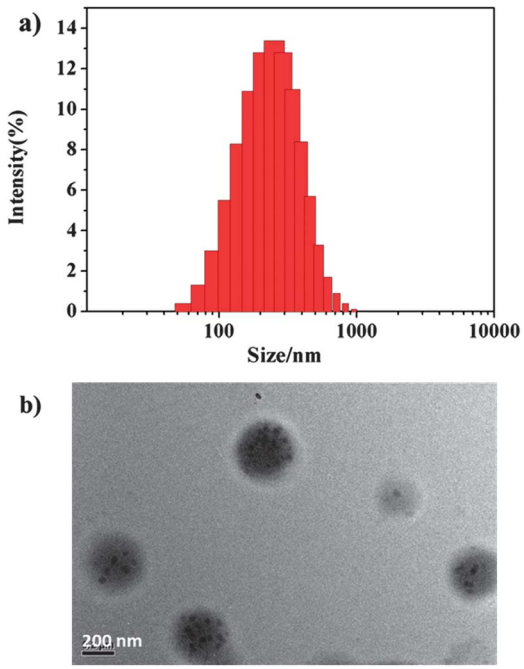

Fig. 7 Size and size distribution of the NIRF prodrug micelle solution (1.0 mg mL^{-1}) determined by (a) DLS and (b) TEM. The micelle solution was prepared by first dissolving the material and then dialysis against water.

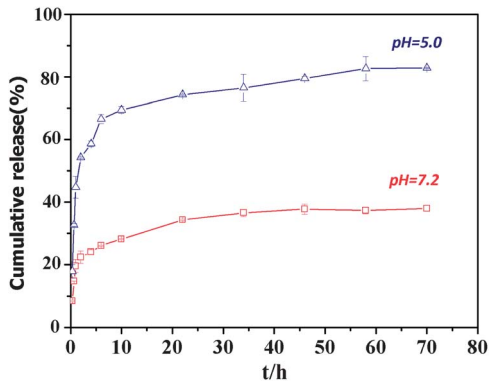

Fig. 8 Drug release behavior of the NIRF prodrug under neutral (pH = 7.2) and acidic (pH = 5.0) conditions.

the polymeric chain was determined to be 8.6% (weight ratio), indicating that each polymeric chain contains one doxorubicin molecule on average. We also found that overfeeding of the drug does not markedly improve drug conjugation but complicates the final product purification, while when a 1 : 1 feed ratio was used, the reaction was qualitative and the purification could be simply accomplished by dialysis.

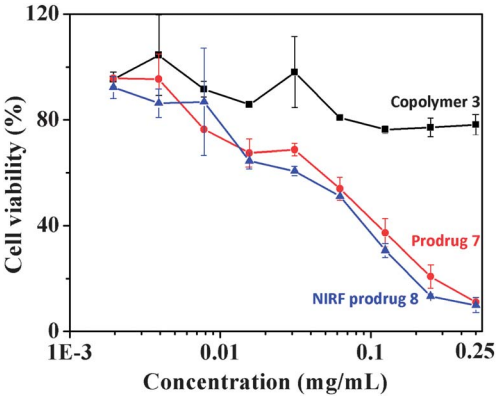

Fig. 9 Toxicity of copolymer **3**, prodrug **7** and NIRF prodrug **8** against A549 cells. A549 cells were incubated with the respective materials for 72 h.

Synthesis of NIRF prodrug 8

For the labeling of macromolecules with cyanine, several methods have been reported in the literature. Direct nucleophilic substitution of the *meso*-position chlorine atom on the central ring with the amine group of the macromolecules is a straightforward method,[37,38] but the validity of this method depends not only on the steric factors resulting from the bulky size of cyanine molecules and macromolecules but also on the nucleophilicity of the amine group. Here in this work, in order to facilitate the labeling, the obtained cyanine dye **5** was first reacted with HOSu to form an activated ester, then prodrug was added to prepare the NIRF prodrug.[44] The ^{1}H NMR spectrum of the obtained fluorescent prodrug was shown in Fig. 5. At a low dye attachment (10% molar ratio), signals corresponding to the dye moiety are barely visible, while when a higher amount (50% molar ratio) of dye is used for labeling, signals of the dye molecules are partially discernable. Signals corresponding to the benzyl group of the dye could be observed at 8.0 ppm, while signals corresponding to the polymethine chain could be observed at 5.9 and 7.5 ppm (overlap with signals of the dye benzyl group).

Optical properties

UV-Vis and fluorescent spectra of the NIRF prodrug aqueous solution were shown in Fig. 6. Characteristic absorption peaks corresponding to the drug and dye moieties could be observed at 488 and 662 nm, while emission peaks corresponding to the drug and the dye were observed at 587 and 725 nm in Fig. 6a and b, respectively. The insets of Fig. 6b show images of the NIRF prodrug micelle solution and its fluorescence image upon excitation at 670 nm. The original light purple solution has strong fluorescence in the near infrared range, confirming its potential applications in the area of bioimaging. Cyanine dye is known to undergo aggregation in both organic and aqueous solutions. Aggregation of the dye molecules either leads to a blue or a red shift of the absorption, depending on H or J form aggregates.[45] In Fig. 6, no absorption other than 662 nm and 488 nm could be observed, indicating that no J and H form aggregation took place. This may be due to a lower number of dye molecules being used for labeling, and the restriction of these molecules to the polymer backbone by chemical bonds, and the chances of

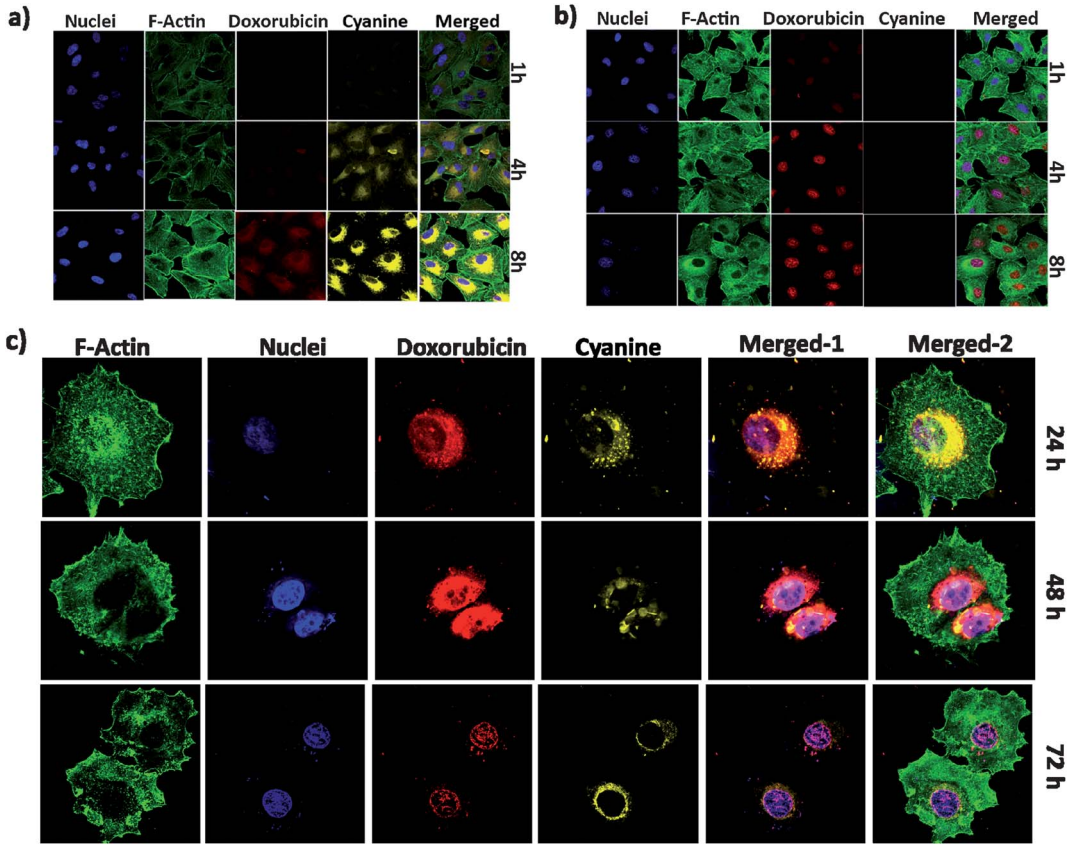

Fig. 10 *In vitro* cellular uptake studies of (a) NIRF prodrug, (b) free doxorubicin at 1 h, 4 h and 8 h. (c) *In vitro* cellular uptake study of the NIRF prodrug at 24, 48 and 72 h. Nuclei: stained blue with DAPI; green: F-actin; red: doxorubicin; yellow: aminocyanine (the original red fluorescence of cyanine was changed to yellow to differ from the fluorescence of doxorubicin).

aggregation were thus greatly reduced. Aminocyanine **5** is hydrophobic, and it is worth noticing that the excitation wavelength of the NIRF prodrug is 662 nm and not in the near infrared range (700–900 nm) in the strictest sense. However, this does not imply that the bioimaging ability of the NIRF prodrug will be markedly reduced, because commercially available NIR dye Cy 5.5, which is widely used for bioimaging, has maximum absorption and emission values of 673 and 692 nm in water.

Quantum yields of NIRF prodrugs with different degrees of dye substitution were listed in Table 2. With the increasing percentage of dye attached, the quantum yield decreases. This may be due to the self-quenching of dye molecules *via* FRET at a higher degree of dye attachment.[46]

Size and size distribution of the obtained nanogel

Size and size distribution of the NIRF prodrug micelle was determined by a combination of TEM and DLS. The results were shown in Fig. 7a and b, respectively. The diameter of the NIRF nanoparticle had an average value of 238 nm, while in the TEM image the diameter of the micelle is an approximate size of around 250 nm.

Drug release behavior of the NIRF prodrug

In vitro drug release behavior of the NIRF prodrug was evaluated under acidic (pH = 5.0) and neutral (pH = 7.2) conditions. The results were shown in Fig. 8. Under neutral conditions, slow drug release was observed in the first 30 h, with no further release during the following 50 h. The total drug release was less than 40% (37%) in the 80 h period, while under acidic conditions an obvious acid promoted drug release behavior was observed. Fast and sustained drug release could be observed during the whole time range, with 80% drug release during the 80 h period. Accelerated drug release may be due to the cleavage of the hydrazone bond under acidic conditions, leading to the release of the conjugated drug.

In vitro cytotoxicity studies

In vitro toxicity of NIRF prodrug **8** was evaluated by a MTT method against the A549 cell. The cell toxicity of copolymer **3** and prodrug **7** were also evaluated as references (Fig. 9). For copolymer **3**, its toxicity upon the A549 cell is low; 80% of the cells were alive after 72 h incubation at a concentration of 0.25 mg mL^{-1}, while for prodrug 7 and NIRF prodrug **8** the toxicity is much more pronounced and increases steadily with concentration of the materials. Only 11% of the cells were alive after 72 h incubation at a concentration of 0.25 mg mL^{-1} for both the NIRF prodrug and the prodrug. Since the difference between copolymer **3** and prodrug **7** is the conjugated doxorubicin, the toxicity of the prodrug could be attributed to conjugated doxorubicin. For the NIRF prodrug and the prodrug, their toxicity

upon the A549 cell was similar, indicating that the aminocyanine's toxicity on the A549 cell is negligible.

Cellular uptake studies

To analyze the internalization and subcellular localization of the NIRF prodrug, cultured A549 cells was treated with the NIRF prodrug (46 μg mL^{-1}) or free doxorubicin (3.3 μg mL^{-1}) of equivalent doxorubicin concentration for 72 h, followed by observation of the cell under confocal laser scanning microscope at different time points (1 h, 4 h, 8 h, 24 h, 48 h and 72 h). To localize the NIRF nanoparticle, the cytoskeleton F-actin was labeled using Alexa 488-phalloidin and the cell nuclei were stained with DAPI. The results were shown in Fig. 10. For cells incubated with free doxorubicin, the fluorescence of doxorubicin at the nucleus was evident even after 1 h of incubation, while almost no signal from the cytoplasm could be observed (Fig. 10b). For the NIRF prodrug, quite distinctive drug transportation and distribution phenomena were observed. The drug signal was dispersed throughout the cell and the signal intensity increases gradually from 1 h to 8 h (Fig. 10a). Since the aminocyanine was conjugated to the NIRF prodrug, the location of the polymeric matrix could be determined by the location of the dye molecules. The gradual increase in the fluorescence intensity of cyanine in the cytoplasm and its overlap with the signal from doxorubicin indicate the gradual endocytosis of the NIRF prodrug. No cyanine fluorescence could be detected in the nucleus, indicating that the polymeric matrix could not enter the nucleus. In order to testify the pH-responsive nature of the NIRF prodrug and confirm its gradual drug release ability *via* pH regulation, the cell culture media containing the NIRF prodrug was replaced with blank culture media after 8 h (in order to eliminate interference from the continued endocytosis NIRF prodrug). The results after 8 h are shown in Fig. 10c. After 24 h incubation, the primarily dispersed doxorubicin fluorescence intensity becomes centralized around the nucleus; the lower fluorescence intensity from the nucleus indicates the migration of the released drug from the NIRF prodrug to the nucleus, while the signal from aminocyanine could only be observed around the nucleus, confirming the drug release properties of the NIRF prodrug. Doxorubicin fluorescence in the nucleus became stronger as time went by. After 72 h incubation, almost no drug signal could be detected in the cytoplasm. Full drug cleavage from the NIRF prodrug had taken place and almost all the drug molecules had migrated into the nucleus, while the polymer matrix remained in the cytoplasm, as indicated by the yellow color from aminocyanine around the nucleus. For free doxorubicin its distribution does not change much after 8 h, and the drug was mainly detected in the nucleus (Fig. S3†). It is worth noticing that the near infrared fluorescence properties of the NIRF polymer do not change too much after 72 h incubation, indicating the potential application of this material as a theranostic agent.

Conclusions

A near infrared fluorescent prodrug with pH-responsive drug release ability was designed and developed. The obtained NIRF prodrug has strong fluorescence in the near infrared range and could release the conjugated drug *via* pH regulation. Sustained drug cleavage from the NIRF prodrug was confirmed by *in vitro* drug release, and further evaluation of the material on A549 cell reveals a gradual drug cleavage and its subsequent migration into the nucleus. With the aid of the NIRF label, the drug–polymer separation process could be conveniently and clearly observed during the 72 h incubation. Due to the excellent drug release behavior of the NIRF prodrug and its unique near-infrared fluorescence properties, the present material has potential applications in biomedical areas as a theranostic agent.

Experimental

Materials

All the chemicals with AR purity, unless specifically indicated, were purchase from Sinoreagent corporation. *n*-Hexane and tetrahydrofuran (THF) were first refluxed with CaH_2 overnight followed by distillation. *N*,*N*-Dimethylformamide (DMF) was dried over CaH_2 at room temperature for 24 h before vacuum distillation. Hydrazine dihydrochloride, triphosgene, doxorubicin hydrochloride, *N*-hydroxysuccinimide (HOSu), *N*,*N*′-dicyclohexyl carbodiimide (DCC), diisopropylethylamine (DIEA), 2,3,3-trimethylbenzoindolenine, 3-bromopropionic acid, β-benzyl L-aspartate, and ε-carbobenzoxy-L-lysine were purchased from Aladdin Corporation, China. Dialysis bag (cutoff M_w = 8000) was obtained from Bomei biotechnology corporation, China. mPEG (M_w = 1900) were purchased from Aldrich and used as received without further purification. Milli-Q water (18.2 MΩ) was prepared using a Milli-Q Synthesis System (Millipore, USA). Normal phase column chromatography was performed using 200–300 mesh silica gel (Yantai institute of chemical engineering, China).

Characterization

^1H NMR spectra were measured on a Bruker AC 300 spectrometer. Deuterated dimethyl sulfoxide (DMSO) or deuterated chloroform containing 0.03 vol% tetramethylsilane (TMS) was used as the solvent. FT-IR spectra were measured on a Bruker EQUINOX 55 Fourier transform infrared spectrometer using the KBr disk method. Molecular weights of the samples were determined by Gel Permeation Chromatography (GPC) equipped with two columns (one Shodex GPC KD-804 column and one guard column) and a refractive index detector (RID-10A). DMF was used as the mobile phase and the measurement was performed at 60 °C at a sample concentration of 3 mg mL^{-1}. Monodispersed polystyrene standards were used for the calibration of M_n, M_w and M_w/M_n. Transmission electron microscopy measurements were performed on a JEOL-2010 microscope with an accelerating voltage of 200 kV. Size and size distribution of the micelle solution were determined by dynamic light scattering (DLS) carried out on a Malvern Zetasizer Nano ZS90 with a He–Ne laser (633 nm) and 90° collecting optics. Measurements were performed at room temperature and the data was analyzed by Malvern Dispersion Technology Software 4.20. Fluorescence measurements were carried out on a Shimadzu RF-5301PC Fluorescence spectrophotometer with excitation and emission slit widths of 5 and 15 nm, respectively. UV-Vis spectra were obtained on a Shimadzu UV-2401 PC Ultraviolet

spectrophotometer. ESI mass spectra were obtained on a LCQ Advantage MAX Spectrometer using methanol solutions of the sample.

The molar extinction coefficient of the sample was determined by Beer's law, based on three separate measurements. The relative fluorescence quantum yield was determined using the following equation:[47]

$$\Phi_{F(x)} = (A_s/A_x)(F_x/F_s)(n_x/n_s)^2\Phi_{F(s)}$$

Where Φ, A and n refer to the quantum yield, absorption and refractive index of the solvents used. F_x stands for the area under emission curve. Subscripts x and s represent sample and stander, respectively. Indocyanine green (ICG) was used as a reference standard, with a quantum yield of 0.078 in MeOH.[48]

Synthesis of parent cyanine dye 4

This material was prepared in 68% yield according to a literature method.[36] In brief, 1-hydroxycarbonylethyl-2,3,3-trimethylbenzoindoleninium bromide (0.42 g, 1.16 mmol) and 2-chloro-1-formyl-3-(hydroxymethylene)cyclohex-1-ene (0.10 g, 0.58 mmol) were dissolved into a mixed solvent of benzene (15 mL) and *n*-butanol (35 mL) in a two-necked flask fitted with a Dean–Stark trap and a condenser. The mixture was heated to 110 °C under a nitrogen atmosphere for 16 h, after which the solvent was removed under vacuum. The obtained green solid was washed with ether and purified by normal phase column chromatography, with a gradient elution from EtOAc to EtOAc/methanol (5 : 1). Removing the solvent after column chromatography yields 0.35 g dye **3** (68% yields) as a deep green solid.

^{1}H NMR (300 MHz, DMSO, δ, ppm): 8.34 (dd, J = 22.4, 11.1 Hz, 4H), 8.09 (t, J = 8.2 Hz, 4H), 7.77 (d, J = 8.7 Hz, 2H), 7.58 (ddd, J = 23.5, 15.4, 7.8 Hz, 4H), 6.40 (t, J = 20.7 Hz, 2H), 4.63 (s, 4H), 3.96 (t, J = 6.1 Hz, 4H), 2.84 (d, J = 38.6 Hz, 8H), 1.95 (s, 16H), 1.57–1.32 (m, 4H), 1.20 (dd, J = 14.2, 6.9 Hz, 4H), 0.76 (t, J = 7.1 Hz, 6H). MS (*m*/*z*, ESI): calcd for $C_{52}H_{60}ClN_2O_4$, 811.3; found, 811.4 $[M-Br^-]^+$. ε = 183 333 $M^{-1}\cdot cm^{-1}$, Φ_F = 0.082. R_f = 0.75 (MeOH : EtOAc = 1 : 6).

Synthesis of aminocyanine dye 5

Cyanine dye **4** (150 mg, 0.17 mmol) and 6-aminocaproic acid (30 mg, 0.23 mmol) were added to 5 mL dry DMF, followed by the addition of 29 μL DIEA (22 mg, 0.17 mmol). The obtained solution was heated to 70 °C and stirred in the dark for 8 h. The solvent was then removed under vacuum, and the obtained deep blue solid was washed with ether and further purified by a column chromatography method with gradient elution from EtOAc to EtOAc/methanol (5 : 1). 100 mg (59% yield) deep blue solid was obtained after removing the solvent under vacuum.

^{1}H NMR (300 MHz, DMSO, δ, ppm): 8.13 (t, J = 13.0 Hz, 2H), 7.96 (dd, J = 8.8, 6.1 Hz, 4H), 7.70 (d, J = 12.1 Hz, 2H), 7.56 (dd, J = 17.2, 8.5 Hz, 4H), 7.38 (dd, J = 16.3, 9.1 Hz, 2H), 5.84 (d, J = 12.9 Hz, 2H), 4.37 (s, 4H), 3.94 (t, J = 6.6 Hz, 4H), 3.76 (s, 2H), 2.78 (t, J = 6.9 Hz, 4H), 2.56 (4H, overlap with the solvent signal), 2.27 (t, J = 7.2 Hz, 2H), 1.95–1.71 (m, 18H), 1.70–1.55 (m, 2H), 1.47–1.36 (m, 4H), 1.26–1.14 (m, 4H), 0.94–0.83 (m, 2H), 0.76 (q, J = 7.3 Hz, 6H). MS (*m*/*z*, ESI): calcd for $C_{58}H_{72}N_3O_6$, 906.4; found, 906.5 $[M-Br^-]^+$. ε = 60 000 $M^{-1}\cdot cm^{-1}$, Φ_F = 0.64. R_f = 0.83 (MeOH : EtOAc = 1 : 6).

Synthesis of LLys-NCA

LLys-NCA was prepared following a literature method.[49] In brief, nepsilon-carbobenzoxy-L-lysine (2.0 g, 7.1 mmol) was suspended in 50 mL dry THF, followed by the addition of a THF solution of triphosgene (2.1 g, 7.1 mmol). The obtained suspension was stirred at 45 °C for 2 h, followed by filtration to remove traces unreacted nepsilon-carbobenzoxy-L-lysine, and the filtrate was collected and crystallized three times from a mixture of THF and hexane to give the anhydride as white crystals (1.6 g, 73% yields).

^{1}H NMR (300 MHz, $CDCl_3$, δ, ppm): 7.48 (s, 5H), 6.75 (s, 1H), 5.42–5.13 (m, 2H), 5.01 (s, 1H), 4.40 (s, 1H), 3.32 (d, J = 5.5 Hz, 2H), 2.23–1.40 (m, 6H).

^{13}C NMR (300 MHz, DMSO, δ, ppm): 171.8, 156.1, 152.0, 137.3, 128.4, 127.8, 65.1, 57.0, 41.3, 31.1, 30.6, 28.7. FT-IR (KBr, thin film, cm^{-1}): 1785, 1854.

Synthesis of Asp-NCA

This material was synthesized according to a similar method with ZLLys-NCA of 75% yield.

^{1}H NMR (300 MHz, $CDCl_3$, δ, ppm): 7.45–7.3 (5H, m, Ar–H), 6.2 (1H, s, NH), 5.2 (2H, s, CH_2), 4.61(1H, t, CH) and 2.85 (2H, t, CH_2). FT-IR (KBr, thin film, cm^{-1}): 1782, 1850.

Synthesis of triblock copolymer 2

To a flame dried and argon purged Schlenk tube, 0.68 g (0.36 mmol) mPEG–NH_2 was added under argon, followed by the addition of 10 mL dry DMF to solubilize the macroinitiator. The obtained solution was precooled in an ice-water bath. A DMF solution (5 mL) containing 0.90 g (3.60 mmol) Asp-NCA was added to the macroinitiator solution. The combined solution was stirred at 0 °C for 3 days. Periodical removal of the generated carbon dioxide was realized by connection of the flask to a vacuum line. 1 mL reaction solution was removed at the end of polymerization for analysis, and a DMF solution containing 1.03 g (3.36 mmol) ZLLys-NCA was subsequently added. The obtained mixture was stirred for another 3 days at 0 °C, followed by precipitation into 100 mL cold ether to separate the product. The obtained white solid was redissolved in 10 mL DMF and further purification was performed by extensive dialysis against water. Removing water by freeze-drying gives 2.0 g product as a white solid (90% yield).

Synthesis of hydrazine functionalized triblock copolymer 3

For the preparation of hydrazine functionalized triblock copolymer **3**, 0.25 g (0.037 mmol) triblock copolymer **2** was dissolved into 5 mL dry DMF, followed by the addition of 0.15 g (1.43 mmol) hydrazine dichloride and 0.50 mL (2.90 mmol) DIEA. The obtained suspension was stirred at 45 °C for 36 h to get a clear solution, and purification was performed by extensive dialysis of the DMF solution against 250 mL water for 48 h. The water was changed every 12 h. Removal of the water by

freeze-drying gives 0.21 g (0.035 mmol) product as a white solid (94% yield).

Synthesis of prodrug 7

For the preparation of prodrug **7**, 50 mg (8.4 μmol) hydrazine functionalized triblock copolymer **3** was dissolved into 5 mL DMF. 4.8 mg doxorubicin hydrochloride (8.3 μmol) was then added to the solution. The obtained red solution was stirred at 45 °C in the dark for 36 h. The obtained DMF solution was sealed into a dialysis bag and further purification was achieved by dialysis. Removal of the water after dialysis by freeze-drying gives 40 mg product as a red powder (75% yield). For the determination of the drug conjugation content, 150 μL (1 mg mL^{-1}) prodrug solution was added to 10 mL concentrated 2 M hydrochloride aqueous solution, and the obtained solution was stirred at room temperature for 1 h to cleave the hydrozone bond. The drug concentration was determined using a fluorospectrophotometer at an emission wavelength of 557 nm, with an excitation wavelength of 480 nm and excitation and emission slit widths of 5 and 10 nm. The drug conjugation content (defined as the ratio of drug weight to prodrug weight) was calculated to be 8.6%.

Synthesis of NIRF prodrug 8

Aminocyanine dye **5** (5.0 mg, 5.1 μmol) was dissolved into 1 mL dry DMF solution, followed by the addition of 1 mL DMF solution containing 0.69 mg HOSu (6.0 μmol) and 1.5 mg DCC (7.3 μmol). The obtained mixture was stirred in the dark for 24 h at room temperature. 90 μL of the above dye solution was removed and added dropwise to a stirred solution of prodrug **7** (30 mg, 4.6 μmol) in DMF. The combined solution was stirred overnight, followed by precipitation into cold ether to separate the NIRF prodrug. Further purification was performed by dialysis of a DMF solution of the NIRF prodrug in the dark. Removal of the water after dialysis by freeze-drying gives 28 mg product as a grey solid (81% yield). The NIRF prodrug with 25% and 50% dye substitution (molar ratio) was prepared in a similar manner.

In vitro drug release

Drug release behavior of the NIRF prodrug was evaluated under both acidic and neutral conditions. For the neutral conditions, 400 μL NIRF prodrug solution (1 mg mL^{-1}) was sealed into a dialysis bag, which was then immersed into 50 mL 0.2 M phosphate buffered saline (PBS) solution; release experiment was conducted at 37 °C on a shaking bath. 2 mL sample was removed at predetermined time points, and 2 mL fresh PBS was added at the same time. Drug release was quantified by using a fluorospectrophotometer at an emission wavelength of 557 nm, with an excitation wavelength of 480 nm. For acidic conditions, a similar method was employed, except that 0.2 M acetate buffer was employed as the release media.

Cytotoxicity

The cytotoxicity of the NIRF prodrug was evaluated with a methyl tetrazolium (MTT) viability assay against the A549 cell. The prodrug and NIRF prodrug micelle solutions were prepared by first dissolving the material into DMF and then removing the organic solvent by dialysis. A549 cells were seeded in a 96-well plate with a cell number of 5000 cells per well. A 1640 solution containing 10% fetal bovine serum (FBS) was used as the cell culture medium. After incubating at 37 °C for 24 h under a 5% CO_2 atmosphere, the culture medium was replaced with a series of material solutions (in 1640 media containing 10% FBS), ranging from 0 to 0.25 mg mL^{-1}. Then the cells were incubated at 37 °C for 3 days, and the culture medium was removed and 100 μL fresh 1640 (10% FBS) was added to each well, followed by the addition of 25 μL MTT stock solution (5 mg mL^{-1}). 100 μL extraction buffer (20% SDS in 50% DMF, pH 4.7, prepared at 37 °C) was added to each well after an additional incubation of 2 h. The obtained solution was incubated overnight, and the absorbance of the solution was measured at 490 nm using a Bio-Rad 680 microplate reader. The cell viability was normalized to A549 cells cultured in the complete culture medium.

Cellular uptake study

A549 cells (7×10^4 cells per well) were seeded on coverslips in 24-well plates and incubated for 24 h. The NIRF prodrug was added to a final concentration of 46 μg mL^{-1} and incubated with the cells for 8 h, after which the culture medium with the NIRF prodrug was replaced with a blank culture medium without the NIRF prodrug, and the incubation was continued for another 64 h. Free doxorubicin was added to a concentration of 3.3 μg mL^{-1} (equivalent to the drug concentration of the NIRF prodrug) and treated by the same method. After removing the medium, the cells were washed twice with cold phosphate buffered saline (PBS, pH 7.4, 0.01 M) and fixed with 4% formaldehyde (Sigma Aldrich, St. Louis, USA). To label the cytoskeleton, the cells were incubated with Alexa Fluor 488-phalloidin (Invitrogen, Carlsbad, USA) at 25 °C for 20 min (after incubation with 1 mg mL^{-1} bovine serum albumin (BSA) in PBS to decrease nonspecific interactions) followed by rinsing with PBS. To label the nucleus, the cells were incubated with 1 mg mL^{-1} DAPI (Beyotime, Haimen, China) for 5 min in PBS, followed by extensive rinsing with PBS. The slides were mounted with one drop of Fluoromount Aqueous Mounting Medium (Invitrogen, Carlsbad, USA) and observed using a Zeiss LSM 710 laser confocal scanning microscope imaging system (Heidenheim, Germany) with an upright confocal microscope and an excitation wavelength of 633 nm.

Acknowledgements

We would like to thank the National Natural Science foundation of China (no. 20874095 and no. 50173147) for the financial support. Professor Jun Wang of USTC is greatly appreciated for both his beneficial discussion with us and his generous help.

Notes and references

1 S. M. Janib, A. S. Moses and J. A. MacKay, *Adv. Drug Delivery Rev.*, 2010, **62**, 1052.
2 M. E. Caldorera-Moore, W. B. Liechty and N. A. Peppas, *Acc. Chem. Res.*, 2011, **44**, 1061.
3 H. Koo, M. S. Huh, I.-C. Sun, S. H. Yuk, K. Choi, K. Kim and I. C. Kwon, *Acc. Chem. Res.*, 2011, **44**, 1018.

4 S. C. Abeylath, S. Ganta, A. K. Iyer and M. Amiji, *Acc. Chem. Res.*, 2011, **44**, 1009.
5 H.-J. Cho, I.-S. Yoon, H. Y. Yoon, H. Koo, Y.-J. Jin, S.-H. Ko, J.-S. Shim, K. Kim, I. C. Kwon and D.-D. Kim, *Biomaterials*, 2012, **33**, 1190.
6 C.-L. Peng, Y.-H. Shih, P.-C. Lee, T. M.-H. Hsieh, T.-Y. Luo and M.-J. Shieh, *ACS Nano*, 2011, **5**, 5594.
7 Y. Matsumura and H. Maeda, *Cancer Res.*, 1986, **46**, 6387.
8 S. Laurent, D. Forge, M. Port, A. Roch, C. Robic, L. V. Elst and R. N. Muller, *Chem. Rev.*, 2008, **108**, 2064.
9 S. Mornet, S. Vasseur, F. Grasset and E. Duguet, *J. Mater. Chem.*, 2004, **14**, 2161.
10 A. Y. Louie, *Chem. Rev.*, 2010, **110**, 3146.
11 X. Michalet, F. F. Pinaud, L. A. Bentolila, J. M. Tsay, S. Doose, J. J. Li, G. Sundaresan, A. M. Wu, S. S. Gambhir and S. Weiss, *Science*, 2005, **307**, 538.
12 X. H. Gao, Y. Y. Cui, R. M. Levenson, L. W. K. Chung and S. M. Nie, *Nat. Biotechnol.*, 2004, **22**, 969.
13 I. L. Medintz, H. T. Uyeda, E. R. Goldman and H. Mattoussi, *Nat. Mater.*, 2005, **4**, 435.
14 X. He, J. Gao, S. S. Gambhir and Z. Cheng, *Trends Mol. Med.*, 2010, **16**, 574.
15 J. V. Frangioni, *Curr. Opin. Chem. Biol.*, 2003, **7**, 626.
16 R. Weissleder, C. H. Tung, U. Mahmood and A. Bogdanov, *Nat. Biotechnol.*, 1999, **17**, 375.
17 B. M. Barth, E. I. Altinoglu, S. S. Shanmugavelandy, J. M. Kaiser, D. Crespo-Gonzalez, N. A. DiVittore, C. McGovern, T. M. Goff, N. R. Keasey, J. H. Adair, T. P. Loughran, Jr, D. F. Claxton and M. Kester, *ACS Nano*, 2011, **5**, 5325.
18 X. Chi, D. Huang, Z. Zhao, Z. Zhou, Z. Yin and J. Gao, *Biomaterials*, 2012, **33**, 189.
19 G. S. Kwon and K. Kataoka, *Adv. Drug Delivery Rev.*, 1995, **16**, 295.
20 H. Otsuka, Y. Nagasaki and K. Kataoka, *Adv. Drug Delivery Rev.*, 2003, **55**, 403.
21 C. D. H. Alarcon, S. Pennadam and C. Alexander, *Chem. Soc. Rev.*, 2005, **34**, 276.
22 D. Schmaljohann, *Adv. Drug Delivery Rev.*, 2006, **58**, 1655.
23 S. Ganta, H. Devalapally, A. Shahiwala and M. Amiji, *J. Controlled Release*, 2008, **126**, 187.
24 J. Kost and R. Langer, *Adv. Drug Delivery Rev.*, 2001, **46**, 125.
25 S. E. Paramonov, E. M. Bachelder, T. T. Beaudette, S. M. Standley, C. C. Lee, J. Dashe and J. M. J. Frechet, *Bioconjugate Chem.*, 2008, **19**, 911.
26 Y.-L. Li, L. Zhu, Z. Liu, R. Cheng, F. Meng, J.-H. Cui, S.-J. Ji and Z. Zhong, *Angew. Chem., Int. Ed.*, 2009, **48**, 9914.
27 L. Zhou, R. Cheng, H. Tao, S. Ma, W. Guo, F. Meng, H. Liu, Z. Liu and Z. Zhong, *Biomacromolecules*, 2011, **12**, 1460.
28 Y. Bae, S. Fukushima, A. Harada and K. Kataoka, *Angew. Chem., Int. Ed.*, 2003, **42**, 4640.
29 F. Wang, Y.-C. Wang, S. Dou, M.-H. Xiong, T.-M. Sun and J. Wang, *ACS Nano*, 2011, **5**, 3679.
30 F. Meng, W. E. Hennink and Z. Zhong, *Biomaterials*, 2009, **30**, 2180.
31 S. Cerritelli, D. Velluto and J. A. Hubbell, *Biomacromolecules*, 2007, **8**, 1966.
32 W. Gao, J. M. Chan and O. C. Farokhzad, *Mol. Pharmaceutics*, 2010, **7**, 1913.
33 K. Kataoka, T. Matsumoto, M. Yokoyama, T. Okano, Y. Sakurai, S. Fukushima, K. Okamoto and G. S. Kwon, *J. Controlled Release*, 2000, **64**, 143.
34 W. K. Moon, Y. H. Lin, T. O'Loughlin, Y. Tang, D. E. Kim, R. Weissleder and C. H. Tung, *Bioconjugate Chem.*, 2003, **14**, 539.
35 H. Lee, W. Akers, K. Bhushan, S. Bloch, G. Sudlow, R. Tang and S. Achilefu, *Bioconjugate Chem.*, 2011, **22**, 777.
36 Z. R. Zhang and S. Achilefu, *Org. Lett.*, 2004, **6**, 2067.
37 C. Ornelas, R. Lodescar, A. Durandin, J. W. Canary, R. Pennell, L. F. Liebes and M. Weck, *Chem.–Eur. J.*, 2011, **17**, 3619.
38 C. Ornelas, R. Pennell, L. F. Liebes and M. Weck, *Org. Lett.*, 2011, **13**, 976.
39 L. Strekowski, M. Lipowska and G. Patonay, *J. Org. Chem.*, 1992, **57**, 4578.
40 X. J. Peng, F. L. Song, E. Lu, Y. N. Wang, W. Zhou, J. L. Fan and Y. L. Gao, *J. Am. Chem. Soc.*, 2005, **127**, 4170.
41 S. A. Hilderbrand, K. A. Kelly, R. Weissleder and C. H. Tung, *Bioconjugate Chem.*, 2005, **16**, 1275.
42 W. Vayaboury, O. Giani, H. Cottet, A. Deratani and F. Schue, *Macromol. Rapid Commun.*, 2004, **25**, 1221.
43 W. Agut, D. Taton and S. Lecommandoux, *Macromolecules*, 2007, **40**, 5653.
44 J. H. Flanagan, S. H. Khan, S. Menchen, S. A. Soper and R. P. Hammer, *Bioconjugate Chem.*, 1997, **8**, 751.
45 A. Mishra, R. K. Behera, P. K. Behera, B. K. Mishra and G. B. Behera, *Chem. Rev.*, 2000, **100**, 1973.
46 K. E. Sapsford, L. Berti and I. L. Medintz, *Angew. Chem., Int. Ed.*, 2006, **45**, 4562.
47 J. N. Demas and G. A. Crosby, *J. Phys. Chem.*, 1971, **75**, 991.
48 R. C. Benson and H. A. Kues, *Phys. Med. Biol.*, 1978, **23**, 159.
49 W. H. Daly and D. Poche, *Tetrahedron Lett.*, 1988, **29**, 5859.

